Thermally assisted Pauli spin blockade in double quantum dots

M. Kondo,[1,*] S. Miyota,[1] W. Izumida,[2] S. Amaha ⍟,[3] and T. Hatano ⍟[1,†]

[1]*College of Engineering, Nihon University, Koriyama, Fukushima 963-8642, Japan*
[2]*Department of Physics, Tohoku University, Sendai, Miyagi 980-8578, Japan*
[3]*RIKEN, Center for Emergent Matter Science, 3-1 Wako, Saitama 351-0198, Japan*

We investigate the influence of thermal energy on the current flow and electron spin states in double quantum dots in series. The quadruplet Pauli spin blockade, which is caused by the quadruplet and doublet states, occurs at low temperatures affecting the transport properties. As the temperature increases, the quadruplet Pauli spin blockade occurs as a result of the thermal energy, even in regions where it does not occur at low temperatures. This is because the triplet state is formed in one dot as a result of the gradual change of the Fermi distribution function of the electrodes with increasing temperature. Moreover, the thermally assisted Pauli spin blockade results in coexistence of the Coulomb and Pauli spin blockades. Conversely, for the standard triplet Pauli spin blockade, which occurs as a result of the triplet and singlet states, the current through the double dots monotonously smears out as the temperature increases. Therefore, the thermally assisted Pauli spin blockade is not clearly observed. However, the coexistence of the Coulomb and triplet Pauli spin blockades as a result of the thermal energy is clearly obtained in the calculation of the probability of the spin state in the double dots.

I. INTRODUCTION

Quantum information processing via nanoscale devices is increasingly attracting attention. Of such nanoscale devices, semiconductor quantum dot devices, which can manipulate electron spins one by one, are expected to be applied to quantum computers [1].

For double quantum dots in series, that are formed by electrostatically and quantum mechanically coupling two quantum dots, when an electron is effectively localized in a quantum dot, the current through the coupled dots is suppressed by the Pauli spin blockade, which forbids transitions between the triplet and singlet states according to the Pauli exclusion principle [2]. The conventional Pauli spin blockade with a spin-triplet state (the triplet Pauli spin blockade) is used for the initialization and readout of a qubit; therefore, the triplet Pauli spin blockade is a key technology in the application of quantum dot quantum computers. The coherent manipulation of single spins [3–6] and two-spin entanglement [7,8] have been reported, and, more recently, a hybrid structure containing a single-spin qubit and a triplet singlet qubit and the high-temperature operation of a silicon qubit have also been reported [9,10]. For double quantum dots in series, the quadruplet state is formed with one conducting and two localized electrons. In this case, the tunneling of the conducting electron is forbidden by Pauli spin exclusion as a result of the quadruplet state and a quadruplet Pauli spin blockade occurs [11].

The Coulomb and Pauli spin blockades are observed with a finite applied source drain voltage. This corresponds to a nonequilibrium system; therefore, it is necessary but difficult to explain the correlation between the electrons in the ground states and the excited electrons, because the current flows not only via the ground state but also via the excited states. Further, because the current suppression can be fundamentally explained by a qualitative discussion of the relationship between the spin states and their energies [12], extensive quantitative studies of the relationship between the current suppression and the properties of the spin states are still not completely understood.

Recently, the relationship between thermal energy and quantum mechanical effects has been intensively studied, and findings concerning the spin Seebeck effect [13] and a quantum heat engine using a single-spin qubit [14] have been reported. Therefore, it is possible to discover new physics with respect to thermal energy and spin via the investigation of the relationship between thermal energy and the Pauli spin blockade.

In this paper, we investigate the current and the probabilities of the spin states of double quantum dots in series at different temperatures around the region where the Coulomb and Pauli spin blockades are observed. As the temperature increases, it is demonstrated that the quadruplet Pauli spin blockade occurs as a result of the thermal energy and that the Coulomb and Pauli spin blockades coexist. Conversely, the triplet Pauli spin blockade is not clearly confirmed in the properties of the current flows. However, for the triplet Pauli spin blockade, the coexistence of the Coulomb and Pauli spin blockades is observed in the properties of the probability of the spin states of the double dots as a result of the thermally assisted Pauli spin blockade. This indicates that the thermal

---

*Present address: Toppan Printing Co., Ltd.
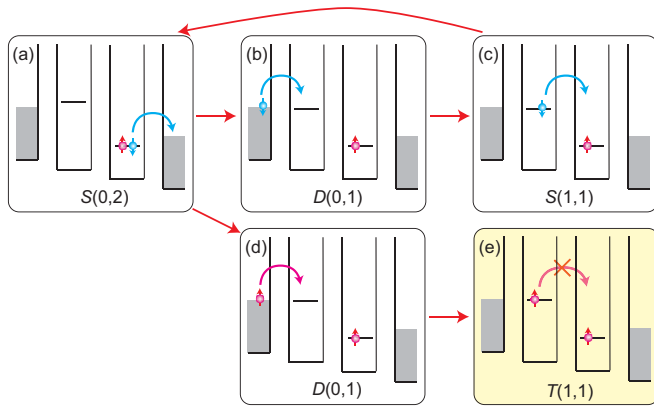†hatano.tsuyoshi@nihon-u.ac.jp

FIG. 1. Schematic of the charge and spin states and their transitions in $(0, 2) \rightarrow (0, 1) \rightarrow (1, 1) \rightarrow (0, 2)$: (a) singlet state $S(0, 2)$, (b) doublet state $D(0, 1)$, (c) singlet state $S(1, 1)$, (d) doublet state $D(0, 1)$, and (e) triplet state $T(1, 1)$. Here, (N_L, N_R) indicates the electron numbers in dots L and R, respectively. There are one and two levels in dots L and R, respectively.

energy enhances the current suppression effect caused by the high-spin states that work as dark states, e.g., the triplet and quadruplet states.

II. CURRENT PROCESS FOR TWO AND THREE LEVELS

First, we discuss the mechanisms of the triplet and quadruplet Pauli spin blockades. The charge transfer process in $(0, 2) \rightarrow (0, 1) \rightarrow (1, 1) \rightarrow (0, 2)$, where the triplet Pauli spin blockade occurs, is shown in Fig. 1. Here (N_L, N_R) indicates the electron numbers in dots L and R, respectively. We start from the state in which two electrons are localized in dot R. Then, the ground state is the singlet state ($S = 0$), $S(0, 2)$, where an electron with up-spin and another with down-spin occupy the lowest single-particle level, as shown in Fig. 1(a). S indicates the total spin quantum number in the double quantum dots.

Suppose that the electron with down-spin tunnels into the drain electrode when a finite value of V_{sd} is applied. Then, the doublet state $D(0, 1)$ is formed, as shown in Fig. 1(b). Here, if the electron with down-spin tunnels into dot L from the source electrode, the singlet state $S(1, 1)$ is realized, as shown in Fig. 1(c). Finally, the electron with down-spin tunnels into dot R and the double-dot state returns to $S(0, 2)$. Therefore, in this case, the current flows through the double quantum dots. Note that this current cycle is correct, even if the roles of the up-spin and down-spin electrons are exchanged. It is assumed that the electron with up-spin in the source electrode tunnels into dot L after the formation of $D(0, 1)$, as shown in Fig. 1(d). Then, the triplet state $T(1, 1)$ is realized, as shown in Fig. 1(e). In this situation, the electron with up-spin in dot L is forbidden from tunneling into dot R according to the Pauli exclusion principle. Therefore, the current through the double quantum dots is suppressed. This indicates that the triplet state works as a dark state.

Next, the charge transfer process in $(0, 3) \rightarrow (0, 2) \rightarrow (1, 2) \rightarrow (0, 3)$, where the quadruplet Pauli spin blockade occurs, is shown in Fig. 2. We start from the state in which three electrons are localized in dot R. Then, the ground state is
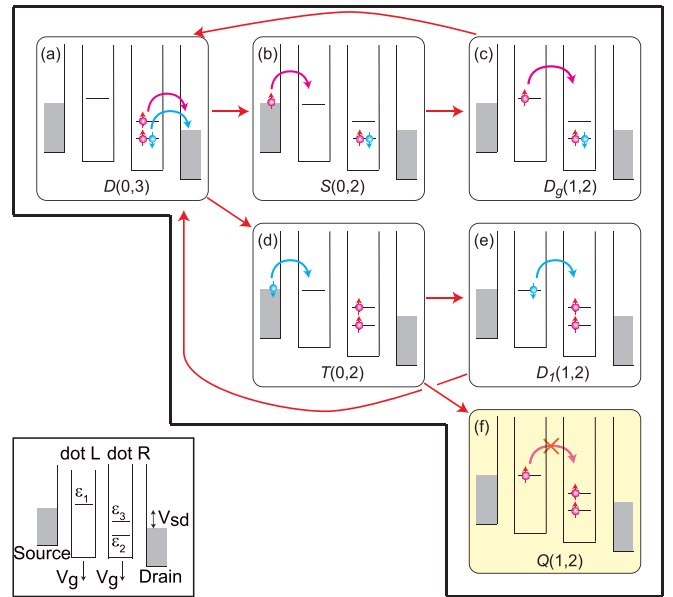

FIG. 2. Schematic of the charge and spin states and their transitions in $(0, 3) \rightarrow (0, 2) \rightarrow (1, 2) \rightarrow (0, 3)$: (a) doublet state $D(0, 3)$, (b) singlet state $S(0, 2)$, (c) doublet state $D_g(1, 2)$, (d) triplet state $T(0, 2)$, (e) doublet state $D_1(1, 2)$, and (f) quadruplet state $Q(1, 2)$. Inset: Energy schematic of the double quantum dots in series used for the calculation.

the doublet state ($S = 1/2$), $D(0, 3)$, where two electrons (one with up-spin and the other with down-spin) and one electron (e.g., with up-spin) occupy the lowest and the second lowest single-particle levels, respectively, as shown in Fig. 2(a).

When low V_{sd} is applied to the double quantum dots, the electron with up-spin, which occupies the second lowest single-particle level in dot R, tunnels into the drain electrode and the singlet state $S(0, 2)$ is formed, as shown in Fig. 2(b). Then, the electron with up-spin tunnels into dot L from the source electrode and the doublet state $D_g(1, 2)$ is realized, as shown in Fig. 2(c). Finally, the electron with up-spin tunnels into dot R and the double-dot state returns to $D(0, 3)$. Therefore, in this case, the current flows through the double quantum dots.

Next, let us consider the case in which a higher V_{sd} is applied to the double quantum dots. Assuming that the electron with up-spin, which occupies the lowest single-particle level in dot R, tunnels into the drain electrode, the electron with up-spin, which occupies the second lowest single-particle level in dot R, transits to the lowest state and the electron state in the double dots becomes $S(0, 2)$, as shown in Fig. 2(b), because of the short relaxation time of an electron with the same spin from the excited state to the ground state [15]. Then, the electron with up- or down-spin tunnels from the source electrode to dot L and the current flows through the double dots. Conversely, when the electron with down-spin, which occupies the lowest single-particle level in dot R, can tunnel into the drain electrode, the triplet state $T(0, 2)$ is realized as the first excited state, as shown in Fig. 2(d). Then, in the case in which the electron with down-spin enters dot L, as shown in Fig. 2(e), the current flows through the double quantum dots. Conversely, when the electron with up-spin enters dot L, the

quadruplet state $Q(1, 2)$ is formed, as shown in Fig. 2(f). In this situation, the electron with up-spin in dot L is forbidden from tunneling into dot R according to the Pauli exclusion principle; therefore, the current through the double quantum dots is suppressed, i.e., the quadruplet Pauli spin blockade occurs [11]. This indicates that the quadruplet state works as a dark state.

III. MODEL AND METHODS

The calculation model of the double dots in series that we use is shown in the inset of Fig. 2. In the double quantum dots, dots L and R are coupled in series and the source and drain electrodes are connected to the two quantum dots. There is one level in dot L and two levels in dot R.

In this paper, we consider the following Hamiltonian:

$$H = H_{DQD} + H_e + H_{e-d},$$

$$
H_{DQD} = \sum_{i=1,\sigma=\uparrow,\downarrow}^{3} (\varepsilon_i - eV_g)n_{i,\sigma} + \sum_{i=1}^{3} U_i n_{i,\uparrow} n_{i,\downarrow}
$$
$$
+ U_{12}n_1 n_2 + U_{23}n_2 n_3 + U_{31}n_3 n_1
$$
$$
+ \sum_{\sigma=\uparrow,\downarrow} (t_{12}a_{1,\sigma}^{\dagger}a_{2,\sigma} + t_{31}^{*}a_{1,\sigma}^{\dagger}a_{3,\sigma} + \text{H.c.}),
$$

$$
H_e = \sum_{k,\sigma=\uparrow,\downarrow} \varepsilon_{s,k}n_{sk,\sigma} + \sum_{k,\sigma=\uparrow,\downarrow} \varepsilon_{d,k}n_{dk,\sigma},
$$

$$
H_{e-d} = \sum_{k,\sigma=\uparrow,\downarrow} vc_{sk,\sigma}^{\dagger}a_{1,\sigma} + \sum_{i=2}^{3}\sum_{k,\sigma=\uparrow,\downarrow} vc_{dk,\sigma}^{\dagger}a_{i,\sigma} + \text{H.c.},
$$

where H_{DQD} describes the electrons in the two quantum dots, H_e describes the electrons in the source and drain electrodes, and H_{e-d} describes the electron tunneling between the two electrodes and the dots. Herein, we consider a single-particle level ($i = 1$) in dot L and two levels (a lower level of $i = 2$ and a higher level of $i = 3$) in dot R. The energy states in the two dots are controlled by applying left and right gate voltages, V_{gL} and V_{gR}, respectively. Here, we assume that this model depicts vertical double quantum dots, because the quadruplet Pauli spin blockade has been observed only in vertical double quantum dots in series [11]. Therefore, we assume $V_{gL} = V_{gR} = V_g$ because V_{gL} and V_{gR} change the energy levels of dots L and R, respectively, nearly equally in vertical quantum double dots. Here e is the elementary charge. Note that the following discussion holds true universally for double quantum dots, even though here we use parameter values that are appropriate for vertical double quantum dots. In addition, $\varepsilon_{i,\sigma}$ ($i = 1, 2, 3$) are the single-particle energies of each level, U_i ($i = 1, 2, 3$) are the intralevel Coulomb energies, U_{ij} ($i = 1, 2, 3, i \neq j$) are the interlevel Coulomb energies, and t_{ij} ($i, j = 1, 2, 3, i \neq j$) are the tunnel coupling energies between the levels. $a_{i,\sigma}$, $a_{i,\sigma}^{\dagger}$, and $n_{i,\sigma}$ ($i = 1, 2, 3, \sigma = \uparrow, \downarrow$) are the annihilation, creation, and electron number operators of the three single-particle levels, respectively, and $\uparrow, \downarrow$ indicate the electron spins. $\varepsilon_{s,k}$ ($\varepsilon_{d,k}$), $c_{sk,\sigma}$ ($c_{dk,\sigma}$), $c_{sk,\sigma}^{\dagger}$ ($c_{dk,\sigma}^{\dagger}$), and $n_{sk,\sigma}$ ($n_{dk,\sigma}$) are the energy, annihilation, creation, and electron number operators with the wave vector k and the spin σ in the source (drain) electrode, respectively. v is the coupling energy
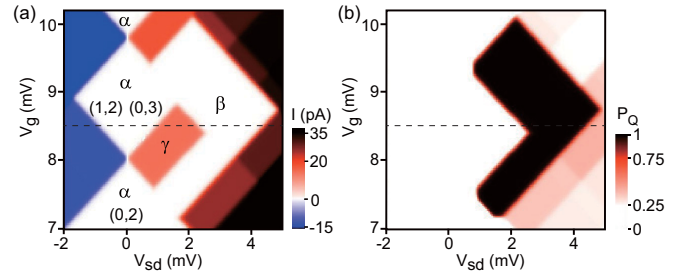

FIG. 3. (a) Intensity plot of the current through the double quantum dots in series: I as a function of the source drain voltage V_{sd} and the gate voltage V_g at a temperature of $T = 300$ mK. (1,2) and (0,3) are the charge configurations in the Coulomb diamond of the total electron number $N = 3$, and (0,2) is the Coulomb diamond of $N = 2$. They are assigned according to the constant interaction model [11,17–20]. (b) Intensity plot of the probability of the quadruplet state, P_Q, as a function of V_{sd} and V_g at $T = 300$ mK.

between the single-particle levels in dot L (R) and the source (drain) electrode. We assume that the source drain voltage V_{sd} symmetrically shifts the electrochemical potentials in the source and drain electrodes, $\mu_s = eV_{sd}/2$ and $\mu_d = -eV_{sd}/2$, respectively.

We diagonalized the Hamiltonian H_{DQD} to solve for the spin states in the double dots, and calculated the current flow accounting for H_e and H_{e-d} in the rate equations. The method to calculate the current flow is derived in the Appendix [16].

The parameters adopted for our calculation are based on a previous experiment [11], and the following values were used: $U_1 = U_2 = U_3 = 3.5$ meV, $U_{12} = 2.1$ meV, $U_{23} = 3.5$ meV, $U_{31} = 1.75$ meV, $t_{12} = 0.035$ meV, $t_{23} = 0$ meV (levels 2 and 3 in the same dot), and $t_{31} = 0.0035$ meV. The coupling strength between the dots and electrodes, γ, was 0.7 μeV (see the Appendix).

IV. QUADRUPLET PAULI SPIN BLOCKADE

To study the influence of the thermal energy on the quadruplet Pauli spin blockade, we considered the three single-particle level model in the inset of Fig. 2. Here, we used the single-particle levels $\varepsilon_1 - \varepsilon_2 = 3.85$ meV, and $\varepsilon_3 - \varepsilon_2 = 0.3$ meV, based on $\varepsilon_2 = 0$ meV. Figure 3(a) shows an intensity plot of the current through the double quantum dots in series I as a function of the source drain voltage V_{sd} and the gate voltage V_g at a temperature of $T = 300$ mK. Similar to the two-level case, the Coulomb staircase is clearly observed because of the sufficiently low temperature and the current flow is suppressed in several regions in Fig. 3(a). The current-suppressed rhombuses [α in Fig. 3(a)] with centers focused on $V_{sd} = 0$ V correspond to the Coulomb blockade regions.

Conversely, the current-suppressed region for positive values of V_{sd}, shown as the β region in Fig. 3(a), is the quadruplet Pauli spin blockade region [11]. Therefore, the quadruplet state works as the dark state. In the region of the rectangular conductive island marked as the γ region in Fig. 3(a), the current flows via $S(0, 2)$, $T(0, 2)$, and $D_g(1, 2)$, $D_1(1, 2)$, or $D(0, 3)$, as indicated in Fig. 2.

Here, we show an intensity plot of the probability of the quadruplet state of the electron state in the double dots being
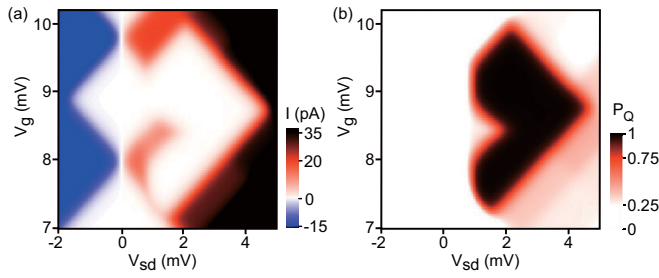
FIG. 4. (a) Intensity plot of I as a function of V_{sd} and V_g at $T = 1$ K. (b) Intensity plot of P_Q as a function of V_{sd} and V_g at $T = 1$ K.

$Q(1, 2)$, P_Q, as a function of V_{sd} and V_g at $T = 300$ mK in Fig. 3(b). The value of P_Q is nearly zero at negative values of V_{sd}. Accordingly, at negative values of V_{sd}, the quadruplet Pauli spin blockade does not occur. Similarly, in the regions corresponding to α and γ in Fig. 3(a), the value of P_Q is nearly zero because the energy necessary to form the quadruplet state is not available. Conversely, the value of P_Q in the region corresponding to β in Fig. 3(a) is nearly unity; therefore, the quadruplet Pauli spin blockade occurs. This shows that the high spin state $Q(1, 2)$ is achieved via the dead-end path (a)$\rightarrow$(d)$\rightarrow$(f) in Fig. 2 and that the current is suppressed as a result of the realization of $Q(1, 2)$. When V_{sd} increases further, the value of P_Q is not unity but is a finite value. In this region, the current can flow via the quadruplet state because two electrons can contribute to the current flow simultaneously [21].

In Fig. 4(a), we show an intensity plot of I as a function of V_{sd} and V_g at $T = 1$ K. Compared to Fig. 3(a), the value of I changes somewhat gradually with V_{sd} and V_g as a result of the increase in the thermal energy. However, the γ region becomes small and the β region, i.e., the quadruplet Pauli spin blockade region, becomes larger than that in Fig. 3(a). We show an intensity plot of P_Q as a function of V_{sd} and V_g at $T = 1$ K in Fig. 4(b). As T increases, the edges of the region of $P_Q \sim 1$ are smeared as a result of the thermal energy compared to that at $T = 300$ mK. However, the region of $P_Q \sim 1$ extends to the regions of the Coulomb blockade (α) and the rectangular conductive island (γ) in Fig. 3(a).

Next, we show an intensity plot of I as a function of V_{sd} and V_g at $T = 3$ K in Fig. 5(a). Compared to Fig. 4(a), the value of I changes more gradually with V_{sd} and V_g as a result of the increase in the thermal energy and the Coulomb blockade region is observed. However, the rectangular conductive
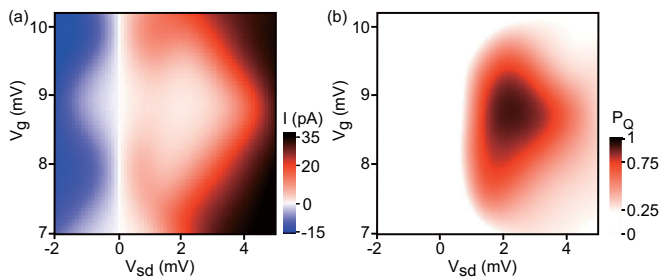

FIG. 5. Intensity plot of I as a function of V_{sd} and V_g at $T = 3$ K. (b) Intensity plot of P_Q as a function of V_{sd} and V_g at $T = 3$ K.
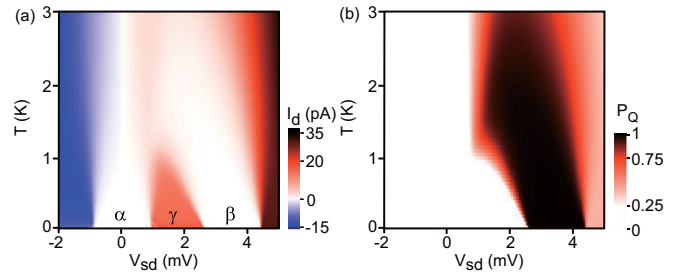

FIG. 6. (a) Intensity plot of I as a function of T and V_{sd} at $V_g = 8.5$ meV. (b) Intensity plot of P_Q as a function of T and V_{sd} at $V_g = 8.5$ meV.

island (γ) in Fig. 3(a) cannot be definitively confirmed. In addition, we show an intensity plot of P_Q as a function of V_{sd} and V_g at $T = 3$ K in Fig. 5(b). As T increases, the region of $P_Q \sim 1$ is even more smeared than at $T = 1$ K as a result of the thermal energy and becomes triangular in shape. Therefore, the Coulomb blockade (α), the quadruplet Pauli spin blockade (β), and the rectangular conductive island (γ) in Fig. 3(a) cannot be distinguished. This indicates that the quadruplet Pauli spin blockade occurs in the region where it does not occur at $T = 300$ mK, i.e., in the α and β regions in Fig. 3(a). Moreover, the Pauli spin and Coulomb blockades coexist in part of the α region in Fig. 3(a) as a result of the thermal energy.

In Fig. 6(a), we show an intensity plot of I as a function of T and V_{sd} at fixed $V_g = 8.5$ mV, to investigate the temperature dependence of the current suppression of I in the γ region in Fig. 3(a). The V_g sweeping direction is indicated by the dashed line in Fig. 3(a), and the α, β, and γ regions correspond to those in Fig. 3(a). As the temperature increases from 0 to 1 K, the γ region abruptly diminishes and the quadruplet Pauli spin blockade region (β) abruptly extends in the direction of the lower values of V_{sd}. Figure 6(b) shows an intensity plot of P_Q as a function of T and V_{sd} at fixed $V_g = 8.5$ mV. Similar to Fig. 6(a), the region of $P_Q \sim 1$ extends in the direction of lower values of V_{sd}, as the temperature increases from 0 to 1 K. Therefore, the quadruplet Pauli spin blockade occurs for lower values of V_{sd} with increasing temperature. This indicates that the thermally assisted quadruplet Pauli spin blockade occurs. For normal semiconductors, as the temperature increases, the quantum mechanical effects become weaker and the properties caused by these effects are smeared. This current suppression with increasing temperature is different from the normal semiconductor-temperature dependence.

To reveal the mechanism of the thermally assisted quadruplet Pauli spin blockade, we show schematic energy diagrams of dot R and the drain electrode at low and high temperatures in Figs. 7(a) and 7(b), respectively. Here, the three-electron state of dot R is $D(0, 3)$, as shown in Fig. 2(a). To generate the quadruplet Pauli spin blockade, it is necessary that the electron with the down-spin tunnels from dot R to the drain electrode and that $T(0, 2)$ is realized as shown in Fig. 2(d). For low temperatures, the Fermi distribution function of the drain electrode abruptly changes near the Fermi energy, as indicated in Fig. 7(a). Accordingly, there are hardly any empty states just below the Fermi energy and the electron with down-spin
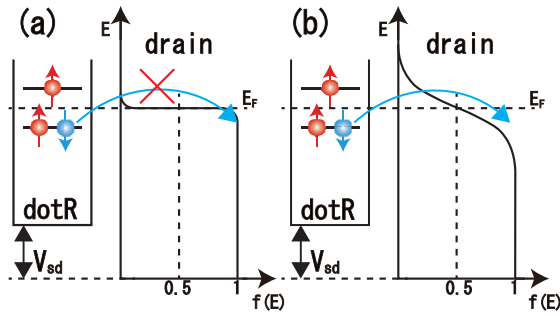
FIG. 7. Energy schematic of the dot R and drain at (a) low and (b) high temperatures.

FIG. 8. (a) Intensity plot of I as a function of V_{sd} and V_g at $T = 100$ mK. (1,1) and (0,2) are the charge configurations in the Coulomb diamond of the total electron number $N = 2$, and (0,1) is the Coulomb diamond of $N = 1$. They are assigned according to the constant interaction model [11,17–20]. (b) Intensity plot of the probability of the triplet state $T(1, 1)$, P_T, as a function of V_{sd} and V_g at $T = 100$ mK.

in dot R is forbidden from tunneling into the drain electrode. A high value of V_{sd} is needed for the electron with down-spin to tunnel from dot R to the drain electrode and to realize $T(0, 2)$; therefore, a high value of V_{sd} needs to be applied to the double quantum dots to cause the quadruplet Pauli spin blockade.

However, as the temperature increases, the Fermi distribution function of the drain gradually changes near the Fermi energy and a large number of empty states exist just below this energy, as indicated in Fig. 7(b). As a consequence, it is possible for an electron with down-spin to tunnel from dot R to the drain electrode and the quadruplet state is realized even for comparatively lower values of V_{sd}. Therefore, assisted by the thermal energy, the quadruplet Pauli spin blockade occurs.

Here, we discuss the difference between the triplet and quadruplet Pauli spin blockades. For the quadruplet Pauli spin blockade, because of the current island located between the Coulomb and quadruplet Pauli spin blockades, it is easy to observe the thermally assisted quadruplet Pauli spin blockade. Conversely, for the triplet Pauli spin blockade, the region of this blockade is adjacent to that of the Coulomb blockade. Therefore, we cannot clearly observe the thermally assisted triplet Pauli spin blockade. In both Pauli spin blockade cases, one can confirm the coexistence of the quadruplet Pauli spin and Coulomb blockades via a measurement of not only the current flow but also the spin states in the double quantum dots.

V. TRIPLET PAULI SPIN BLOCKADE

How does the thermal energy affect the triplet Pauli spin blockade? We consider a model in which there is one single-particle level in each dot. Here, we assume $\varepsilon_1 - \varepsilon_2 = 1.05$ meV and $\varepsilon_3 - \varepsilon_2 = 350$ meV based on $\epsilon_2 = 0$ meV for the calculation model in the inset of Fig. 2. Then, the energy level ϵ_3 can be excluded because it is much larger than the applied V_{sd} and V_g. Figure 8(a) shows an intensity plot of I as a function of V_{sd} and V_g at $T = 100$ mK. The Coulomb staircase is clearly observed because of the sufficiently low temperature, and the current flow is suppressed in several regions. The Coulomb blockade (α) and triplet Pauli spin blockade (β) regions are confirmed in Fig. 8(a) [2]. Note that the property of I is symmetric with respect to $V_g = 4.35$ mV as a result of the electron-hole symmetry.

To investigate the electron states of the double dots in the region where the current is suppressed, we show an intensity
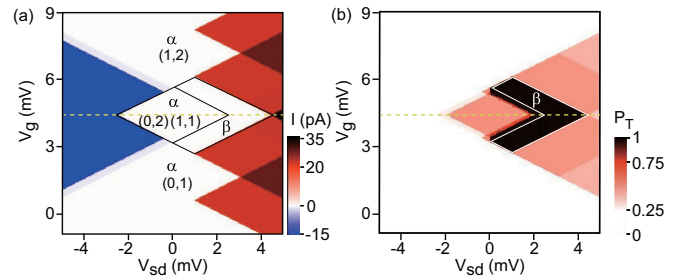
plot of the probability of the triplet state of the electron state in the double dots being $T(1, 1)$, P_T, as a function of V_{sd} and V_g at a temperature of $T = 100$ mK in Fig. 8(b). The β region, where the triplet Pauli spin blockade occurs, is surrounded by a white line and corresponds to the triplet Pauli spin blockade region in Fig. 8(a). The value of P_T is nearly unity for the β region. This shows that the high-spin state $T(1, 1)$ is achieved via the dead-end path (a)→(d)→(e) in Fig. 1 and that the current is suppressed as a result of the realization of $T(1, 1)$. For the α region, where the Coulomb blockade occurs, P_T has a nonzero finite value, even though $T(1, 1)$ is the excited state [22]. This is because a finite value of V_{sd} is applied, i.e., this system is in nonequilibrium. Further, the region of $P_T \sim 1$ extends into the edge of the α region at $V_{sd} > 0$ in Fig. 8(a); therefore, in the region of $P_T \sim 1$ in the Coulomb blockade region, the triplet Pauli spin blockade coincides with the Coulomb blockade.

In Fig. 9(a), we show an intensity plot of I as a function of V_{sd} and V_g at $T = 3$ K. Compared to Fig. 8(a), the value of I gradually changes with V_{sd} and V_g as a result of the increase in the thermal energy. The current suppression regions, the Coulomb and triplet Pauli spin blockades, are observed. Here, we show an intensity plot of P_T as a function of V_{sd} and V_g at $T = 3$ K in Fig. 8(b). As T increases, the edges of the region of $P_T \sim 1$ are smeared as a result of thermal energy compared to those at $T = 100$ mK. However, P_T is nearly unity for $V_{sd} > 0$ mV in the α region in Fig. 8(a), as opposed to P_T in Fig. 8(b). This shows that the high-spin state $T(1, 1)$
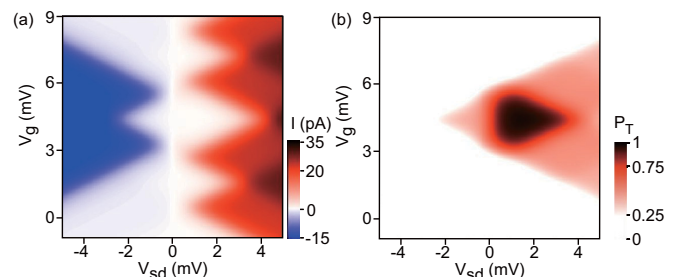

FIG. 9. (a) Intensity plot of I as a function of V_{sd} and V_g at $T = 3$ K. (b) Intensity plot of P_T as a function of V_{sd} and V_g at $T = 3$ K.

is achieved in the region for $V_{sd} > 0$ mV in the Coulomb blockade region as the temperature increases. This indicates that the dead-end path (a)→(d)→(e) in Fig. 1 is caused by the thermal energy and that the Coulomb and Pauli spin blockades coexist. Therefore, in the region of $P_T \sim 1$ in the Coulomb blockade region, the simple Coulomb blockade does not occur; however, an electron is forbidden from tunneling through dot R as a result of both the Coulomb repulsion and the Pauli exclusion principle in the double dots. However, this cannot be observed from the properties of I; to confirm this, the spin state in the double quantum dots needs to be detected.

VI. CONCLUSIONS

We calculated the current and spin states in double quantum dots in series. As the temperature increases, the quadruplet Pauli spin blockade occurs as a result of the thermal energy. The triplet Pauli spin blockade is not clearly confirmed in the properties of the current flows. However, for both Pauli spin blockades, the coexistence of the Coulomb and Pauli spin blockades occurs as a result of the thermally assisted Pauli spin blockade and is reflected in the properties of the probability of the spin states of the double dots. This coexistence affects the initialization and readout of qubits in quantum dot quantum computing and may reduce the qubit fidelity. Moreover, in nanoscale devices, heat transport and dissipation have become important topics [23], e.g., the operation temperatures of quantum devices and quantum computing [10] and a single-quantum-dot heat valve [24]. Therefore, our results pave a way toward the clarification of spin-based transport and thermal excitation in nanoscale devices, and it may also be possible to realize novel quantum devices, e.g., quantum heat engines [14], using the thermally assisted Pauli spin blockade.

APPENDIX: DETAILS OF CALCULATIONS

We describe the calculation method of the probability of the quadruplet and triplet states, P_Q and P_T, respectively, and the current flow, I. It is assumed that the coupling between two quantum dots is relatively strong, and that the coupling between the double quantum dot and two electrodes is a sequential tunneling process [25]. Therefore, we diagonalize the Hamilton H_{DQD} and obtain the eigenvalues and eigenvectors of H_{DQD}. The eigenvectors can be indicated by $N(= N_L + N_R)$ and S, which are the total electron and total spin numbers in the double quantum dot, respectively, because N and S are conserved quantities for H_{DQD}. In Table I, we show the basis vectors to use for the digitalization of H_{DQD}, corresponding to the eigenvectors of H_{DQD} at $t_{1i} = t_{i1}^* = 0$ ($i = 2, 3$). Therefore, the eigenvectors of H_{DQD} are expressed by a linear combination of the basis vectors.

TABLE I. Basis vectors to diagonalize H_{DQD}. $N(= N_L + N_R)$ and S indicate the total electron numbers and total spin quantum number in the double quantum dots, respectively. $|\xi_1, \xi_2, \xi_3\rangle$ represents the occupation of the single-particle energy levels, and ξ_i denotes the local states, 0, ↑, ↓, and ↑↓, which stand for empty, spin states up and down of the occupied electrons, and two electron occupation. σ indicates ↑ or ↓, and $\bar{\sigma}$ represents ↓ (↑) for σ =↑ (↓).

N	S	Basis vectors
0	0	$\|0, 0, 0\rangle$
1	$\frac{1}{2}$	$\|\sigma, 0, 0\rangle, \|0, \sigma, 0\rangle, \|0, 0, \sigma\rangle$
2	0	$\|\uparrow\downarrow, 0, 0\rangle, \|0, \uparrow\downarrow, 0\rangle, \|0, 0, \uparrow\downarrow\rangle, \frac{1}{\sqrt{2}}(\|\uparrow, \downarrow, 0\rangle - \|\downarrow, \uparrow, 0\rangle)$ $\frac{1}{\sqrt{2}}(\|0, \uparrow, \downarrow\rangle - \|0, \downarrow, \uparrow\rangle), \frac{1}{\sqrt{2}}(\|\uparrow, 0, \downarrow\rangle - \|\downarrow, 0, \uparrow\rangle)$
2	1	$\|\sigma, \sigma, 0\rangle, \|0, \sigma, \sigma\rangle, \|\sigma, 0, \sigma\rangle, \frac{1}{\sqrt{2}}(\|\uparrow, \downarrow, 0\rangle + \|\downarrow, \uparrow, 0\rangle)$ $\frac{1}{\sqrt{2}}(\|0, \uparrow, \downarrow\rangle + \|0, \downarrow, \uparrow\rangle), \frac{1}{\sqrt{2}}(\|\uparrow, 0, \downarrow\rangle + \|\downarrow, 0, \uparrow\rangle)$
3	$\frac{1}{2}$	$\|\sigma, 0, \uparrow\downarrow\rangle, \|0, \sigma, \uparrow\downarrow\rangle, \|0, \uparrow\downarrow, \sigma\rangle$ $\|\sigma, \uparrow\downarrow, 0\rangle, \|\uparrow\downarrow, \sigma, 0\rangle, \|\uparrow\downarrow, 0, \sigma\rangle$ $\frac{1}{\sqrt{2}}(\|\sigma, \uparrow, \downarrow\rangle - \|\sigma, \downarrow, \uparrow\rangle)$ $\frac{1}{\sqrt{6}}(\|\sigma, \uparrow, \downarrow\rangle + \|\sigma, \downarrow, \uparrow\rangle - 2\|\bar{\sigma}, \sigma, \sigma\rangle)$
3	$\frac{3}{2}$	$\|\sigma, \sigma, \sigma\rangle, \frac{1}{\sqrt{3}}(\|\uparrow, \uparrow, \downarrow\rangle + \|\uparrow, \downarrow, \uparrow\rangle + \|\downarrow, \uparrow, \uparrow\rangle)$ $\frac{1}{\sqrt{3}}(\|\downarrow, \downarrow, \uparrow\rangle + \|\downarrow, \uparrow, \downarrow\rangle + \|\uparrow, \downarrow, \downarrow\rangle)$
4	0	$\|\uparrow\downarrow, \uparrow\downarrow, 0\rangle, \|\uparrow\downarrow, 0, \uparrow\downarrow\rangle, \|0, \uparrow\downarrow, \uparrow\downarrow\rangle$ $\frac{1}{\sqrt{2}}(\|\uparrow\downarrow, \uparrow, \downarrow\rangle - \|\uparrow\downarrow, \downarrow, \uparrow\rangle)$ $\frac{1}{\sqrt{2}}(\|\uparrow, \uparrow\downarrow, \downarrow\rangle - \|\downarrow, \uparrow\downarrow, \uparrow\rangle)$ $\frac{1}{\sqrt{2}}(\|\uparrow, \downarrow, \uparrow\downarrow\rangle - \|\downarrow, \uparrow, \uparrow\downarrow\rangle)$
4	1	$\|\uparrow\downarrow, \sigma, \sigma\rangle, \|\sigma, \uparrow\downarrow, \sigma\rangle, \|\sigma, \sigma, \uparrow\downarrow\rangle$ $\frac{1}{\sqrt{2}}(\|\uparrow\downarrow, \uparrow, \downarrow\rangle + \|\uparrow\downarrow, \downarrow, \uparrow\rangle)$ $\frac{1}{\sqrt{2}}(\|\uparrow, \uparrow\downarrow, \downarrow\rangle + \|\downarrow, \uparrow\downarrow, \uparrow\rangle)$ $\frac{1}{\sqrt{2}}(\|\uparrow, \downarrow, \uparrow\downarrow\rangle + \|\downarrow, \uparrow, \uparrow\downarrow\rangle)$
5	$\frac{1}{2}$	$\|\sigma, \uparrow\downarrow, \uparrow\downarrow\rangle, \|\uparrow\downarrow, \sigma, \uparrow\downarrow\rangle, \|\uparrow\downarrow, \uparrow\downarrow, \sigma\rangle$
6	0	$\|\uparrow\downarrow, \uparrow\downarrow, \uparrow\downarrow\rangle$

Thereafter, we calculate the transition probability from the initial spin state, $|i\rangle$, to the final spin state, $|f\rangle$, in the double quantum dot, $\Gamma_{fi}^{s(d)}$, corresponding to the coupling strength between the double quantum dot and source (drain) electrode, as follows:

$$\Gamma_{fi}^{s(d)} = \frac{2\pi}{\hbar} \sum_{I,F} |\langle F|\langle f|H_{e-d}|i\rangle|I\rangle|^2 W_I \delta(E_{fF} - E_{iI}). \quad (A1)$$

Here $|I\rangle$ and $|F\rangle$ are the initial and final states in the source (drain) electrode, respectively. $|i\rangle$ and $|f\rangle$ are the eigenvectors of H_{DQD} and are denoted using N and S. W_I is the probability that the initial state in the source (drain) electrode is $|I\rangle$ under thermal equilibrium. E_{iI} and E_{fF} are the total energies of the initial and final states of the double quantum dot and two electrodes, respectively. $\Gamma_{fi}^{s(d)}$ is nonzero for $N_f = N_i \pm 1$ and is numerically obtained in our calculation. N_i and N_f are the numbers of electrons in the double quantum dot for $|i\rangle$ and $|f\rangle$, respectively.

As an example, we show Γ_{21}^s, corresponding to the transition probability from the initial spin state $|1\rangle$ to the final state

$|2\rangle$. $|1\rangle$ is the state in which there are no electrons in the double quantum dot, and $|2\rangle$ is the state in which there is one electron in the double quantum dot, as follows:

$$|1\rangle = |0, 0, 0\rangle,$$

$$|2\rangle = A|\uparrow, 0, 0\rangle + B|0, \uparrow, 0\rangle + C|0, 0, \uparrow\rangle,$$

where A, B, and C are coefficients ($|A|^2 + |B|^2 + |C|^2 = 1$). Therefore, Γ_{21}^s is calculated as follows:

$$\Gamma_{21}^s = \frac{2\pi}{\hbar}|\langle 2|H_{e-d}|1\rangle|^2 W_I \delta(E_{fF} - E_{iI})$$

$$= \frac{2\gamma}{\hbar} f_s(E_2 - E_1)|A|^2, \qquad (A2)$$

where $\gamma = \pi v^2 \sum_k \delta(E_2 - E_1 - \varepsilon_{sk})(= \pi v^2 \sum_k \delta(E_2 - E_1 - \varepsilon_{dk}))$ is the tunneling strength between the source electrode and the double quantum dot. $f_s(E_2 - E_1)$ is the Fermi distribution function in the source electrode, and E_2 and E_1 are the eigenvalues of $|2\rangle$ and $|1\rangle$, respectively. $\varepsilon_{s(d)k}$ is the energy of the source (drain) electrode. Similarly, we define $f_d(\varepsilon_{dk})$ as the Fermi distribution function in the drain electrode.

In addition, we define the transition probability from $|i\rangle$ to $|f\rangle$, Γ_{fi}, which is contributed to by tunneling between the source electrode to the double quantum dot and by tunneling between the drain electrode and the double quantum dot, as follows:

$$\Gamma_{fi} = \Gamma_{fi}^s + \Gamma_{fi}^d. \qquad (A3)$$

We denote the probability of the eigenvector $|i\rangle$ as $P(i)$, and with Γ_{fi}, the rate equation is expressed as follows:

$$\frac{d}{dt}P(i) = \sum_j (\Gamma_{ij}P(j) - \Gamma_{ji}P(i)), \qquad (A4)$$

with the normalization condition $\sum_i P(i) = 1$. We solve Eq. (A4) under the stationary condition ($dP(i)/dt = 0$), and the probabilities of the spin state, $P(i)$, are obtained. P_Q and P_T in the main text correspond to $P(i)$ of $Q(1, 2)$ and $T(1, 1)$, respectively.

Finally, the current I is described as follows [25]:

$$I = -e \sum_i \left(\sum_{\substack{j \\ (N_j = N_i + 1)}} \Gamma_{ji}^s P(i) - \sum_{\substack{k \\ (N_k = N_i - 1)}} \Gamma_{ki}^s P(i) \right). \qquad (A5)$$

In the main text, we define the current flow from the source electrode to the drain electrode as positive [11].

[1] D. Loss and D. P. DiVincenzo, Phys. Rev. A **57**, 120 (1998).

[2] K. Ono, D. G. Austing, Y. Tokura, and S. Tarucha, Science **297**, 1313 (2002).

[3] F. H. L. Koppens, C. Buizert, K. J. Tielrooij, I. T. Vink, K. C. Nowack, T. Meunier, L. P. Kouwenhoven, and L. M. K. Vandersypen, Nature (London) **442**, 766 (2006).

[4] E. A. Laird, C. Barthel, E. I. Rashba, C. M. Marcus, M. P. Hanson, and A. C. Gossard, Phys. Rev. Lett. **99**, 246601 (2007).

[5] K. C. Nowack, F. H. L. Koppens, Yu. V. Nazarov, and L. M. K. Vandersypen, Science **318**, 1430 (2007).

[6] M. Pioro-Ladrière, T. Obata, Y. Tokura, Y.-S. Shin, T. Kubo, K. Yoshida, T. Taniyama, and S. Tarucha, Nat. Phys. **4**, 776 (2008).

[7] J. R. Petta, A. C. Johnson, J. M. Taylor, E. A. Laird, A. Yacoby, M. D. Lukin, C. M. Marcus, M. P. Hanson, and A. C. Gossard, Science **309**, 2180 (2005).

[8] R. Brunner, Y.-S. Shin, T. Obata, M. Pioro-Ladrière, T. Kubo, K. Yoshida, T. Taniyama, Y. Tokura, and S. Tarucha, Phys. Rev. Lett. **107**, 146801 (2011).

[9] A. Noiri, T. Nakajima, J. Yoneda, M. R. Delbecq, P. Stano, T. Otsuka, K. Takeda, S. Amaha, G. Allison, K. Kawasaki, Y. Kojima, A. Ludwig, A. D. Wieck, D. Loss, and S. Tarucha, Nat. Commun. **9**, 5066 (2018).

[10] K. Ono, T. Mori, and S. Moriyama, Sci. Rep. **9**, 469 (2019).

[11] S. Amaha, W. Izumida, T. Hatano, S. Tarucha, K. Kono, and K. Ono, Phys. Rev. B **89**, 085302 (2014).

[12] R. Hanson, L. P. Kouwenhoven, J. R. Petta, S. Tarucha, and L. M. K. Vandersypen, Rev. Mod. Phys. **79**, 1217 (2007).

[13] K. Uchida, S. Takahashi, K. Harii, J. Ieda, W. Koshibae, K. Ando, S. Maekawa, and E. Saitoh, Nature **455**, 778 (2008).

[14] K. Ono, S. N. Shevchenko, T. Mori, S. Moriyama, and F. Nori, Phys. Rev. Lett. **125**, 166802 (2020).

[15] A. G. Huibers, M. Switkes, C. M. Marcus, K. Campman, and A. C. Gossard, Phys. Rev. Lett. **81**, 200 (1998).

[16] J. Fransson and M. Råsander, Phys. Rev. B **73**, 205333 (2006).

[17] S. Amaha, W. Izumida, T. Hatano, S. Teraoka, S. Tarucha, J. A. Gupta, and D. G. Austing, Phys. Rev. Lett. **110**, 016803 (2013).

[18] T. Ota, K. Ono, M. Stopa, T. Hatano, S. Tarucha, H. Z. Song, Y. Nakata, T. Miyazawa, T. Ohshima, and N. Yokoyama, Phys. Rev. Lett. **93**, 066801 (2004).

[19] A. Fuhrer, L. E. Fröberg, J. N. Pedersen, M. W. Larssen, A. Wacker, M.-E. Pistol, and L. Samuelson, Nano Lett. **7**, 243 (2007).

[20] S. Amaha, T. Kodera, T. Hatano, K. Ono, Y. Tokura, S. Tarucha, J. A. Gupta, and D. G. Austing, J. Phys. Soc. Jpn. **80**, 023701 (2011).

[21] T. Hatano, Y. Tokura, S. Amaha, T. Kubo, S. Teraoka, and S. Tarucha, Phys. Rev. B **87**, 241414(R) (2013).

[22] Finite values of P_T and P_Q depend on the alignment of the parameters in the double dot, e.g., single-particle energy levels, and intralevel and interlevel Coulomb energies.

[23] E. Pop, Nano Res. **3**, 147 (2010).

[24] B. Dutta, D. Majidi, N. W. Talarico, N. Lo Gullo, H. Courtois, and C. B. Winkelmann, Phys. Rev. Lett. **125**, 237701 (2020).

[25] H. Bruus and K. Flensberg, *Many-Body Quantum Theory in Condensed Matter Physics: An Introduction* (Oxford University Press, Oxford, UK, 2004).